Environmental Pollution 284 (2021) 117163

Contents lists available at ScienceDirect

Environmental Pollution

journal homepage: www.elsevier.com/locate/envpol

Exposure to nanoparticles derived from diesel particulate filter equipped engine increases vulnerability to arrhythmia in rat hearts

Stefano Rossi [a, b, 1], Andrea Buccarello [c, 1, 2], Cristina Caffarra Malvezzi [a], Silvana Pinelli [a], Rossella Alinovi [a], Amparo Guerrero Gerboles [a], Giacomo Rozzi [a, d], Fabio Leonardi [e], Valentina Bollati [f], Giuseppe De Palma [g], Paola Lagonegro [h, 3], Francesca Rossi [h], Pier Paolo Lottici [i], Diana Poli [j], Rosario Statello [a, k], Emilio Macchi [b, c], Michele Miragoli [a, b, d, l, *]

[a] Department of Medicine and Surgery, University of Parma, Parma, Italy
[b] CERT, Center of Excellence for Toxicological Research, University of Parma, Parma, Italy
[c] Department of Chemistry, Life Sciences and Environmental Sustainability, University of Parma, Parma, Italy
[d] Humanitas Clinical and Research Center -IRCCS, 20090, Rozzano, Milan, Italy
[e] Department of Veterinary Science, University of Parma, Parma, Italy
[f] EPIGET Lab, Department of Clinical Sciences and Community Health, Università Degli Studi di Milano, Milano, Italy
[g] Department of Medical and Surgical Specialties, Radiological Sciences, and Public Health, University of Brescia, Brescia, Italy
[h] National Research Council (CNR), Istituto Dei Materiali per L'Elettronica Ed Il Magnetismo (IMEM), Parma, Italy
[i] Department of Mathematical, Physical and Computer Sciences, University of Parma, Parma, Italy
[j] INAIL Research, Department of Occupational and Environmental Medicine, Epidemiology and Hygiene, 00078, Monte Porzio Catone, Rome, Italy
[k] Department of Medical Sciences and Public Health, University of Cagliari, Cagliari, Italy
[l] National Research Council (CNR), Istituto di Ricerca Genetica e Biomedica (IRGB), Milan, Italy

ARTICLE INFO

Article history:
Received 5 March 2021
Received in revised form
12 April 2021
Accepted 14 April 2021
Available online 20 April 2021

Keywords:
Diesel particulate filter
Air pollution
Nanoparticles
Oxidative stress
Arrhythmias
Nanotoxicity

ABSTRACT

Air pollution is well recognized as a central player in cardiovascular disease. Exhaust particulate from diesel engines (DEP) is rich in nanoparticles and may contribute to the health effects of particulate matter in the environment. Moreover, diesel soot emitted by modern engines denotes defective surfaces alongside chemically-reactive sites increasing soot cytotoxicity. We recently demonstrated that engineered nanoparticles can cross the air/blood barrier and are capable to reach the heart. We hypothesize that DEP nanoparticles are pro-arrhythmogenic by direct interaction with cardiac cells. We evaluated the internalization kinetics and the effects of DEP, collected from Euro III (DEPe3, in the absence of Diesel Particulate Filter, DPF) and Euro IV (DEPe4, in the presence of DPF) engines, on alveolar and cardiac cell lines and on *in situ* rat hearts following DEP tracheal instillation. We observed significant differences in DEP size, metal and organic compositions derived from both engines. DEPe4 comprised ultrafine particles (<100 nm) and denoted a more pronounced toxicological outcome compared to DEPe3. In cardiomyocytes, particle internalization is fastened for DEPe4 compared to DEPe3. The *in-vivo* epicardial recording shows significant alteration of EGs parameters in both groups. However, the DEPe4-instilled group showed, compared to DEPe3, a significant increment of the effective refractory period, cardiac conduction velocity, and likelihood of arrhythmic events, with a significant increment of membrane lipid peroxidation but no increment in inflammation biomarkers. Our data suggest that DEPe4, possibly due to ultrafine nanoparticles, is rapidly internalized by cardiomyocytes resulting in an acute susceptibility to cardiac electrical disorder and arrhythmias that could accrue from cellular toxicity. Since the postulated transfer of nanoparticles from the lung to myocardial cells has not been investigated it remains open

* Corresponding author. Dipartimento di Medicina e Chirurgia Via Gramsci, n°14 43126, Parma, Italy.
E-mail address: michele.miragoli@unipr.it (M. Miragoli).
[1] Equally contributed to this work.
[2] Now at the Department of Physiology, University of Bern, Switzerland.
[3] Now at the Italian National Research Council | CNR ·Istituto di Scienze e Tecnologie Chimiche "Giulio Natta" (SCITEC)_Via Alfonso Corti 12, 20133 Milano.

https://doi.org/10.1016/j.envpol.2021.117163
0269-7491/© 2021 Elsevier Ltd. All rights reserved.

whether the effects on the cardiovascular function are the result of lung inflammatory reactions or due to particles that have reached the heart.

© 2021 Elsevier Ltd. All rights reserved.

Abbreviation list

DEP	Diesel Exhaust Particles
DEPe3	Diesel Exhaust Particles derived from EuroIII engines
DEPe4	Diesel Exhaust Particles derived from EuroIV engines
DPF	Diesel Particulate Filter
Ip	Intraperitoneal
PM	Particulate Matter
SEM	Scanning Electron Microscopy
FBS	Fetal Bovine Serum
3MA	3-methyl adenine
TBARS	Thiobarbituric acid reactive substances
EG	Electrogram
ERP	Effective Refractory Period
CVl	Longitudinal Conduction Velocity
CVt	Transverse Conduction Velocity
NIST	National Institute of Standards and Technology
BTEX	Benzene, Toluene, Ethylbenzene and Xylenes
MPPD	Multiple-Path Dosimetry model
TWA	Total-Weight Average

1. Introduction

Particulate Matter (PM) pollution is recognized as an important trigger for cardiovascular disease in urban communities. Inhalation of PM leads to pulmonary inflammation and cardiotoxicity via secondary systemic effects (Iodice et al., 2018; Mills et al., 2009). Four million deaths are attributable to PM < 2.5 μm and nearly 60% of these are related to cardiovascular diseases (Cohen et al., 2017). Similarly, it has been shown that exposure to PM is still associated with the incidence of coronary events in Europe even if the limit value was set at 50 $\mu g/m^3$ daily (Cesaroni et al., 2014). Brief exposure to air pollution has been associated with angina, myocardial infarction, arrhythmia, and heart failure (Bhatnagar, 2006; Brook et al., 2003; Dockery et al., 1993; Mann et al., 2002; Mills et al., 2009; Peters et al., 2001; Samet et al., 2000). Particulate Matter is responsible for the black smokes traditionally associated with diesel-powered vehicles and Diesel Exhaust Particulate (DEP) matter is subject to regulation worldwide; transport activities contribute 20–25% of total anthropogenic emissions of carbonaceous particles (Cofala et al., 2007).

Exhaust particulate from diesel engines is rich in nanoparticles and, therefore, may contribute greatly to the health effects of PM in urban environments (Baulig et al., 2003; Lucking et al., 2011). DEPs are considered “dangerous” because of their high density, small respirable aerodynamic diameter, large surface area, and potential physicochemical interaction with cell membranes. In this regards, it has been hypothesized that newer diesel engines equipped with diesel particulate filter (DPF) emit more nanoparticles with reduced aerodynamic size (Steiner et al., 2016) and such could be more harmful to human health than older engines because nanoparticles may penetrate the lung more deeply (Su et al., 2008) and can translocate to the heart (Miragoli et al., 2018; Nemmar et al., 2002; Steiner et al., 2016). Experimentally, it has been shown that DEPs induce heart rate variability changes, vasoconstriction (Peretz et al., 2008a; 2008b) cardiac mitochondrial dysfunction (Karoui et al., 2019), arterial hypertension (Liu et al., 2018), cardiomyocyte dysfunction in utero (Tanwar et al., 2017) and arrhythmias (Hazari et al., 2011). Despite recent European Union legislation aimed at reducing DEP with the introduction of DPF from Euro IV engines, the health benefits are not tangible (Weitekamp et al., 2020). Notwithstanding the considerable amount of investigations the mechanisms by which DEP jeopardizes cardiac physiology are still undefined, taking into account that the presence of DPF may release more ultrafine particles (Mayer et al., 2014). Here we dissected the mechanisms by which DEPs from Euro3 (DEPe3, absence of DPF) and Euro4 (DEPe4, presence of DPF) differ in internalization kinetics from pulmonary and cardiac cells line *in-vitro* and how such differences may exacerbate cardiac biophysical activity and arrhythmia vulnerability in *in-vivo* animal models.

2. Material and methods

2.1. Particle suspension

DEPs, as a model of ultra-fine particulate matter, were collected by extracting the soot from the surface of the exhaust pipe as suggested by Uy et al. (2014). The two types of DEP were collected immediately after turning on for 5 min and off the engines from Euro III (DEPe3, n = 2 engines) and Euro IV (DEPe4, n = 2 engines, presence of DPF) as described from (Fox et al., 2015). All engines have traveled for >100.000 km DEPe3 and DEPe4 were suspended in a solution containing 0.9% NaCl (10 mg/mL, stock solution).

Before the experiments, the suspension was first vortexed then sonicated (Branson Ultrasonics, Danbury, CT, USA) for 10 min at 37 °C to minimize particle aggregation.

2.2. DEP physicochemical characterization

2.2.1. Organic composition obtained via Raman and gas-chromatography-Mass Spectrometry

Raman Spectroscopy for DEPe3 and DEPe4 samples has been performed using the 632.8 nm line of a 20 mW Melles Griot He-Ne laser as excitation and the back-scattered light was analyzed by a LabRam Jobyn-Yvon micro-Raman spectrometer (Horiba, Japan) equipped with 1800 lines/mm holographic grating and a Peltier cooled CCD detector (1024 × 256 px.). Organic molecules present in DEPe3 and DEPe4 have been evaluated via an HP 6890 gas chromatography coupled with an HP 5973 mass selective detector (Agilent Technologies, Palo Alto, CA, USA) after solid-phase microextraction.

2.2.2. Particle size obtained via Scanning Electron Microscope (SEM)

Sample dimensional analysis was performed by SEM, consisting of a dual-beam Zeiss Auriga Compact system equipped with a GEMINI Field-Effect SEM column and a Gallium Focused Ion Beam (FIB) source (Zeiss). The SEM analysis was performed at 5 keV. The particle size analysis has been obtained by ImageJ 1.52e.

2.2.3. Metal composition obtained via Inductively Plasma-coupled Mass Spectrometry

The collected material was dissolved in hyperpure concentrated nitric acid (Sigma) and then diluted with bidistilled water (Fluka). The reactive white consisted of virgin membranes, acid and the same bidistilled water. The calibration curve was obtained using the external standard method (Multi-Element Calibration Standard 3, PerkinElmer). The solutions obtained were injected into an inductively plasma-coupled mass spectrometer (Elan, DRC II, PerkinElmer), with a dynamic reaction cell for chromium and vanadium. The certified reference material NIST 1643f (National Institute of Standards and Technology, USA) was used to check the accuracy of the method. The detection limit and the coefficient of variation were between 0.0001 and 0.0006 μg and between 6.5 and 9%, respectively. For each sample, a single multi-elemental analysis was performed. The analyses were performed following the best available practices for metal analysis. All experiments have been performed blinded by operators. A detailed methodology is provided in the Supplementary material section.

2.3. In-vitro experiment

2.3.1. Cell culture

A549 alveolar basal epithelial cells were cultured in RPMI 1640 medium supplemented with 10% heat-inactivated Fetal Bovine Serum (FBS, Gibco, Thermofisher, IT), 100U penicillin ml^{-1} and 100 μg streptomycin ml^{-1}, 2 μM l-glutamine and incubated at 37 °C with humidified air containing 5% CO_2. HL-1 cardiomyocytes (Merck, IT) were cultured in Claycomb media (Merck, IT) on 0.02% gelatin and 1 mg/ml fibronectin pre-coated plastic dishes supplemented with heat-inactivated FBS (10%) and norepinephrine (0.1 mM). Exponentially growing cells were used for all assays. Both cell lines were seeded to a concentration of 7×10^4 cells/ml and were incubated for 24h before the treatment with DEP (range of concentration: from 0.5 to 100 μg/ml). We considered untreated cells as control.

2.3.2. Cell proliferation/viability assays

Viability and cytotoxicity of A549 cells and HL-1 cardiomyocytes treated with DEP were determined by three different assays: i) ApoTox-Glo™ Triplex Assay, ii) CytoTox-One™ Homogeneous Membrane Integrity Assay and iii) CellTiter-Glo Luminescent Cell Viability Assay, following the manufacturer's instructions. Luminescence/fluorescence was detected by a Cary Eclipse fluorescence spectrophotometer (Varian, Inc., Palo Alto, CA, USA). We normalized the data against control values. Cells were counted in a Burker hemocytometer. Experiments with DEP were repeated after pre-treatment of cells with 5 mM 3-methyl adenine (3MA) as an autophagy blocker.

2.3.3. Clonogenic survival assay

Exponentially growing A549 and HL-1 cells were diluted to reach an appropriate plating density, seeded in 6-well plates and allowed to adhere overnight. After the addition of increasing concentrations of DEP, cells were cultured for 10 days. Colonies were fixed with methanol/acetic acid (3:1) and stained with crystal violet (0.5% w/v in methanol). Colonies consisting of 50 cells or more were counted using the Fluor-S MultiImager (Bio-Rad, Hercules, CA, USA). The surviving fraction was calculated relative to the mean plating efficiency of untreated control cells. Experiments with DEP were repeated after pre-treatment of cells with 5 mM 3MA.

2.4. In-vivo experiments

2.4.1. Experimental animals

Experiments were conducted on twenty-six 12-week old Sprague Dawley male rats singly housed with a 12-h light cycle (lights on at 19.00h) in a temperature-controlled room at 20–24 °C with food and water available *ad libitum*. This study was carried out following the recommendations in the Guide for the Care and Use of Laboratory Animals of the National Institute of Health (Bethesda, MD, USA, revised 1996), the European Guideline on animal experiments (Directive 2010/63/EU). The protocol was approved by the Veterinary Animal Care and Use Committee of the University of Parma (Permit: 281/2017-PR and PMS 53/2009).

2.4.2. Intra-tracheal instillation

Animals were anesthetized intraperitoneally (Ip) with a mixture of ketamine chloride 40 mg/kg (Imalgene, Merial, Milano, Italy) and medetomidine hydrochloride 0.15 mg/kg (Domitor, Pfizer Italia S.r.l., Latina, Italy). Rats were divided into 3 groups:

i) Physio (N = 10): intratracheal instillation of saline solution;
ii) DEPe3 (N = 8): intratracheal instillation of saline solution + DEPe3 at [2 mg/kg];
iii) DEPe4 (N = 11): intratracheal instillation of saline solution + DEPe4 at [0.7 mg/kg] (n = 3, data not shown) and [2 mg/kg] (n = 8).

Details regarding the prepared solution are provided in the supplemental section.

2.4.3. Epicardial measurements

Epicardial measurement has been acquired by multiple lead electrode arrays as previously described (Rossi et al., 2019). Technical details are provided in the supplemental section.

2.4.4. ROS-induced lipid peroxidation and inflammation in-vivo

Frozen tissue samples were homogenized and sonicated in phosphate-buffered saline supplemented with a protease inhibitor cocktail (Sigma-Aldrich, St. Louis, MO, USA). Insoluble debris was pelleted and lipid peroxidation products were detected in the

supernatants by the Thiobarbituric acid reactive substances (TBARS) method, based on the condensation of malondialdehyde derived from polyunsaturated fatty acids, with two equivalents to give a fluorescent red derivative. TBARS concentrations were normalized to total protein concentration in each sample, determined by the bicinchoninic acid Protein Assay (Thermo Scientific, Rockford, IL, USA). Through enzyme-like immunosorbent assays (Cloud-Clone Corp., Katy, TX, USA) we evaluated biomarkers of tissue inflammation (IL-6 and MCP-1), and tissue remodeling (MMP9, TIMP-1). Inflammation data are related to protein concentration.

2.5. Computational analysis of deposited doses

We employed the Multiple-Path Dosimetry model −MPPD-(https://www.ara.com/mppd/) (Wu et al., 2021) for evaluating the alveolar DEP depositions (ranging from 0.001 μm to 0.1 μm) in humans exposure scenario at 5 mg/m^3, 8-h total-weight-average. Furthermore, we compared these values with DEP depositions derived from i) the endotracheal instilled rats scenario at 2 mg/kg and ii) in-vitro scenario on alveolar monolayer exposed to 50 μg/ml of DEPe3 and DEPe4. Technical details are provided in the supplemental section.

2.6. Statistical analysis

Data were expressed as median and interquartile range or as mean ± standard error of the mean. The normal distribution of variables was checked using the Kolmogorov-Smirnov test. Statistics of variables included unpaired Student's t-test, two-way ANOVA (post hoc analyses: Bonferroni test or Games-Howell test, when appropriate) and Kruskal-Wallis (post hoc analyses: Dunn's multiple comparisons). Prism 5.0 software (GraphPad Software) was used to assess the normality of the data and for statistical calculation. The details on the specific test used for each experiment are reported in the figure legends. P values of <0.05 were considered to be significantly different.

3. Results

3.1. DEPe3 and DEPe4 characterization

The analysis of the Raman spectra has been performed through a 4-peak deconvolution 2L-2G: two Lorentzian profiles (D and G bands) and 2 Gaussian profiles (D_3 and D_4 bands) (Lapuerta, 2019). Examples of the deconvolution of DEPe3 and DEPe4 samples and a Table of the peak positions are reported in Fig. 1A. We observed that both DEPe3 and DEPe4 have an irregular spherical shape, with a noteworthy tendency to form agglomerations of several dozen nanoparticles (Fig. 1B). We found three morphological types: individual particles which are the primary particles generated from diesel engines; small aggregates in the form of chains or clusters; large agglomerates. No macroscopic differences were observed between DEPe3 and DEPe4. Moreover, there is a wide variety of shapes and sizes, as well as a finely porous structure (Fig. 1B). We observed a small size of the DEPe4 (average dimensional distribution of <150 nm) compared to the DEPe3 (<500 nm). It can also be observed that DEPe3 particles <150 nm were absent.

We then sought to investigate the metal content in DEPe3 and DEPe4 soot (Fig. S1A). In DEPe3 Chromium was 64% of total metal content followed by Nickel (14%), Aluminum (8%) Cuprum (6%) and Zinc (5%). Differently, in DEPe4 soot, the major component was Zinc with 48%, followed by Chromium (31%), Nickel (8%), Aluminum (7%) and Cuprum (3%). Organic composition denotes the presence of aromatic hydrocarbons (Benzene, Toluene, Ethylbenzene and Xylenes, BTEX) and polycyclic aromatic hydrocarbons (PAHs. Fig. S1B). Generally, DEPe3 shows higher concentrations of organic compounds (0.006−0.7 μg/g) than DEPe4 (0.002−0.3 μg/g) with an increase from 10% for Naphthalene to 750% for Xylenes. In DEPe3 Xylenes concentration is 41% of total BTEX and PAHs followed by Toluene (18.5%), Naphthalene (17.2%) and Benzene (5%) while in DEPe4 the major component is Naphthalene (36%) followed by Toluene (29%), Xylenes (11%) and Benzene (9%).

3.2. Cellular activity in the presence of DEPe3 and DEPe4

3.2.1. Cellular uptake, viability and proliferation

A549 and HL-1 cells were exposed to increasing concentrations (0.5−100 μg/ml) of DEPe3 and DEPe4. The number of live cells was counted after 24 h. Data expressed as a percentage of control (not exposed to DEP, Fig. 2A−B). Both treatments with DEP had similar effects on lungs and cardiac cell lines: significant decreases in the number of live cells are present only at higher concentrations (50 and 100 μg/ml for A549 cells or 100 μg/ml for HL-1 cells), without any apparent phenomena of lysis or apoptosis (data not shown). The cellular incorporation of DEPe3 and DEPe4 (50 μg/ml, 15.79 μg/cm^2 per well (Table S1) resulted in a 50% increase in SSC in both cell lines after 24 h, albeit with different internalization kinetics. The mean side scatter of A549 cells grows regularly over time (Fig. 2C), whereas in HL-1 cardiomyocytes the early increase within 4 h is significantly pronounced, followed by a plateau (Fig. 2D). This result was also confirmed by the absence in both lines of significant activation of Caspase 3 (data not shown). The clonogenic test showed a decrease in the number of colonies in cultured cells treated with both DEP. This effect is particularly noticeable and significant for the A549, while it is much more limited in HL-1 (Fig. 2E−F). The cytostatic effect was also confirmed by the cell cycle analysis wherein an accumulation of G0/G1 cells was observed at the expense of the other phases in both cell lines studied (Fig. 2G−H). Even for this aspect DEPe3 and DEPe4 show similar behaviors.

3.2.2. Cellular function/activity

To assess the capacity of DEP to generate oxidative stress, the total ROS and TBARS levels were measured. The results obtained in flow cytometry using DCFH-DA probes revealed that both nanoparticles caused a high intracellular production of oxygen species in both A549 and HL-1 cells (Figs. S2A−B). The unusual appearance of two peaks in treated HL-1 cells may be determined by the presence of different clones in the culture (Figs. S2C−D) (Dias et al., 2014). Oxidative stress also provoked lipid peroxidation, highlighted by significant increases in TBARS (Figs. S2E−F) in both cell lines after DEPe3 and DEPe4 treatments.

3.3. In-vivo cardiac electrophysiological and toxicological analysis

3.3.1. Cardiac EG intervals

Durations of the EG waveforms and intervals measured in DEP treated animals were compared to the Physio group (Fig. 3, Table S2). Specifically, DEPe3 treated animal displayed i) reduction in the atrial activation time duration (P wave, Fig. 3A), ii) prolongation of atrioventricular conduction time (PQ segment, Fig. 3B), iii) ventricular repolarization duration (RT interval, QT interval, T wave and QTc. Fig. 3E-F and 3H-I). DEPe4 treated animal displayed a slight tachycardia (RR interval) compared to Physio (Fig. 3G). No changes have been detected for the activation time interval (Fig. 3C).

3.3.2. Cardiac refractoriness

All the values related to cardiac refractoriness were increased in

A

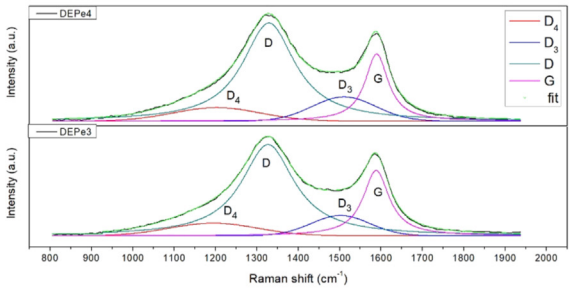

Sample	D	G	D_3	D_4	I_D/I_G
DEPe3	1327±2	1588±2	1502±7	1194±8	2.4±0.2
DEPe4	1329±2	1590±2	1510±8	1203±9	3.1±0.2

B

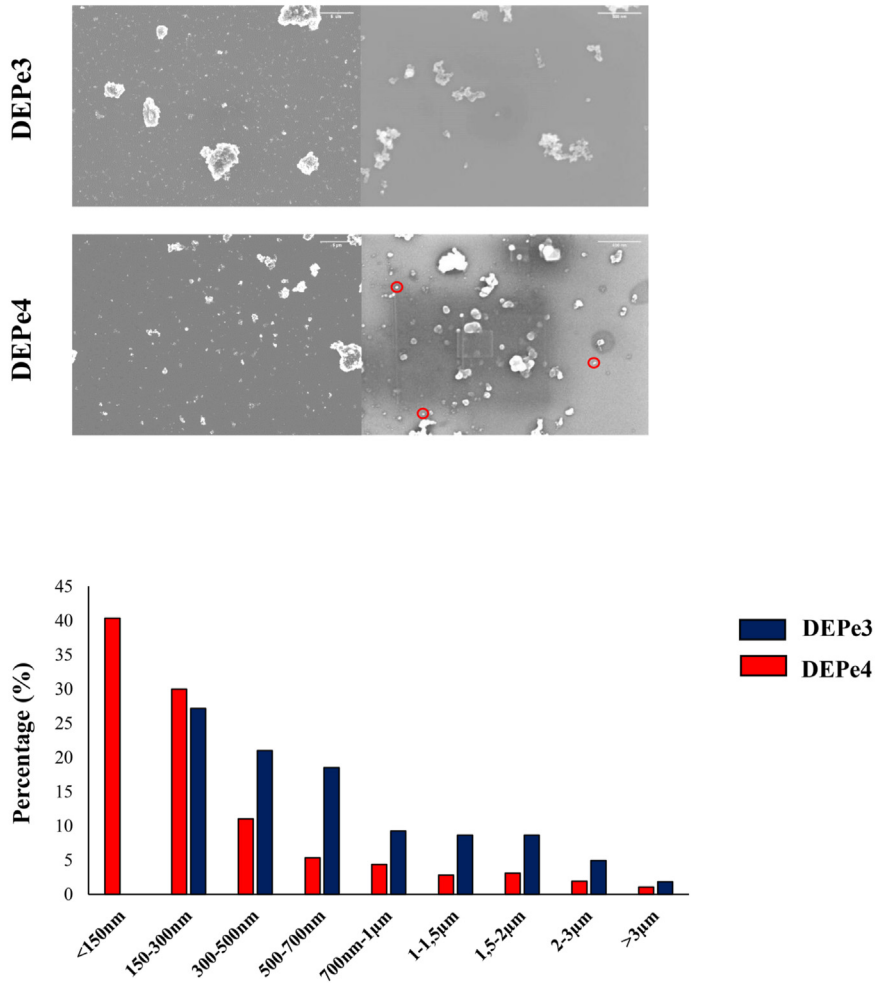

Fig. 1. DEP characterization. **A**. Left. Deconvolution with D, G, D_3 and D_4 sub-bands of the Raman spectra of DEPe3 and DEPe4. Right. The table indicates the peak position (in cm^{-1}) of the bands used for the deconvolution by four bands fitting (2L-2G) of the Raman spectra of DEPe3 and DEPe4 and, in the last column, values of the I_D/I_G parameter. The band labeling is taken from (Sadezky et al., 2005). **B.** Top: Scanning Electron micrographs of diesel exhaust soot from DEPe3 (upper panels) and DEPe4 (lower panels) engines. Red circles indicate the nanoparticles in DEPe4 samples. Bottom: Particle size distribution for DEPe3 (blue) and DEPe4 (red). (For interpretation of the references to colour in this figure legend, the reader is referred to the Web version of this article.)

both DEP treated groups but only statistically significant in DEPe4 animals (Fig. 4A and B). In detail, ventricular Effective Refractory Period (ERP) was not only prolonged by 14% (Physio: 72.2 ± 0.9 ms vs. DEPe4: 82.1 ± 2.4 ms) but its dispersion (we considered SD of the ventricular ERP as dispersion index) was increased by about 69% (Physio: 5.4 ± 0.6 ms vs. DEPe4: 9.1 ± 1.5 ms). During the S1-S2 protocol for ERP evaluation, we also evaluated the percentage of arrhythmia induction measuring how many electrodes recorded, at

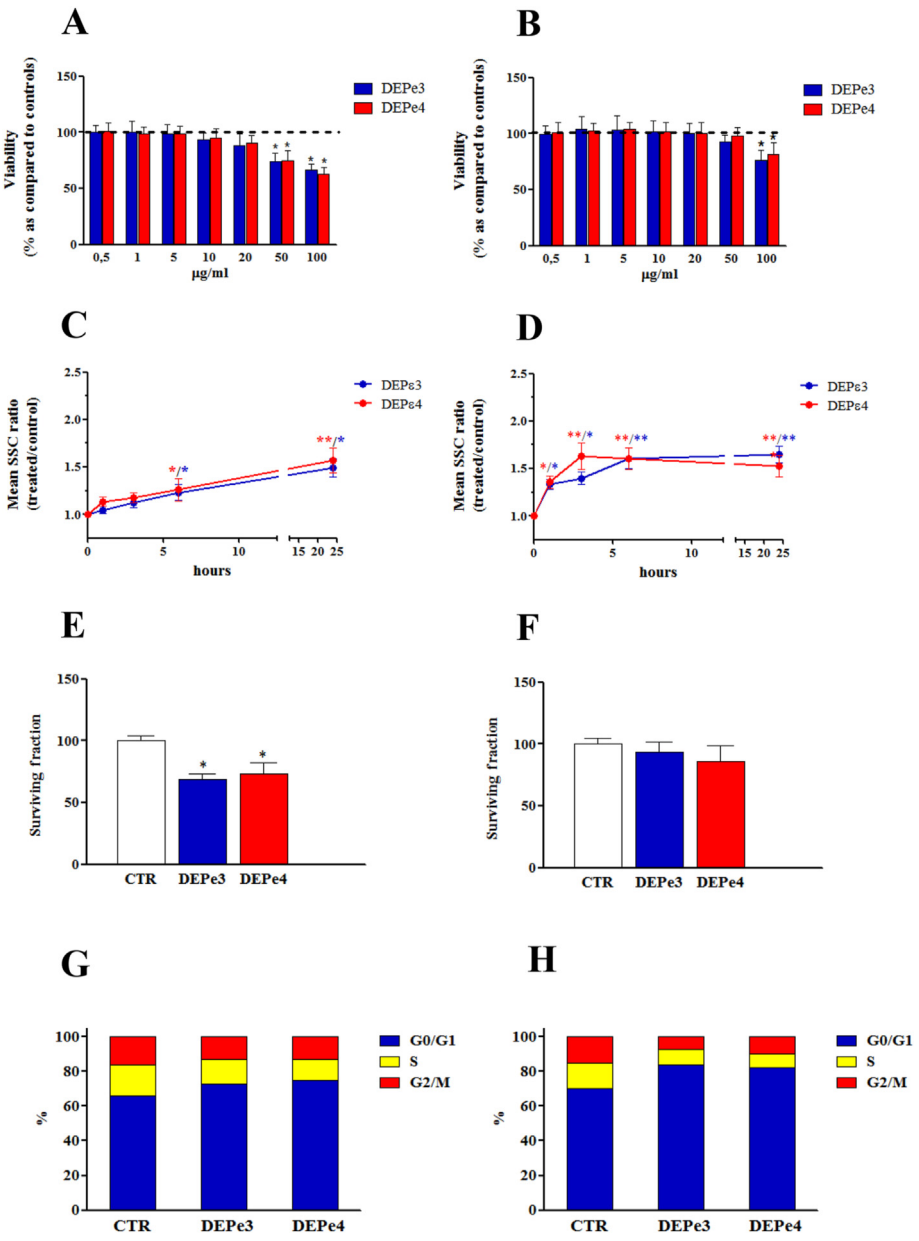

Fig. 2. Multiple cellular parameters. **A** and **B**: Cellular viability after 24h of DEPe3 (blue) and DEPe4 (red) administration in A549 and HL-1 cells, respectively. **C** and **D**: Cellular uptake of DEPe3 (red trace) and DEPe4 (blue trace) in A549 and HL-1 cells, respectively. **E** and **F**: 10-days Cellular survival for control (CTR, white), DEPe3 (blue), and DEPe4 (red) administration in A549 and HL-1 cells, respectively. **G** and **H**: Cell cycle after 24h of DEPe3 and DEPe4 administration in A549 and HL-1 cells, respectively. Statistical significance set at $p < 0.05$. (For interpretation of the references to colour in this figure legend, the reader is referred to the Web version of this article.)

least, one ectopic beat. Arrhythmia susceptibility was nearly doubled in DEPe4 animals (DEPe3: 18% vs. DEPe4: 38%).

3.3.3. Cardiac excitability

Ventricular excitability was reduced, highlight by a shift upward and rightward of the strength-duration curve. Precisely, cardiac excitability decreased in DEPe4 demonstrated by an increase of 40% in Rheobase (Physio: 26.1 ± 1.7 µA vs. DEPe4: 36.5 ± 3.2 µA) and by 65% in Chronaxie (Physio: 0.98 ± 0.07 ms vs. DEPe4: 1.62 ± 0.15 ms) values as displayed in Fig. 4C and D. This result was confirmed by an increase of 55% in the mean threshold of an impulse of 1 ms duration (Physio: 45.6 ± 2.9 µA vs. DEPe4: 70.5 ± 5.3 µA) as displayed in Fig. 4E.

3.3.4. Cardiac conduction velocity

Longitudinal ventricular conduction velocity (CVl) was significantly increased for DEPe4 whereas no differences in transverse ventricular conduction velocity (CVt) were observed in both groups (Fig. 4G). Interestingly the anisotropy ratio (CVl/CVt) was significantly increased only for DEPe4 treated animals Fig. 4H. Specifically, CVl was increased by 8% (Physio: 0.61 ± 0.01 m/s vs. DEPe4: 0.66 ± 0.01 m/s).

All the values regarding the spatial inhomogeneity in the ventricular conduction velocity were reported in Fig. S3. The absolute inhomogeneity in conduction, described by percentile scores and expressed as p05-p95, increased by 71% in DEPe4 and by 48% vs. DEPe3. Moreover, the inhomogeneity index independent of the average conduction velocity (p05-p95/p50) increased by 32% in

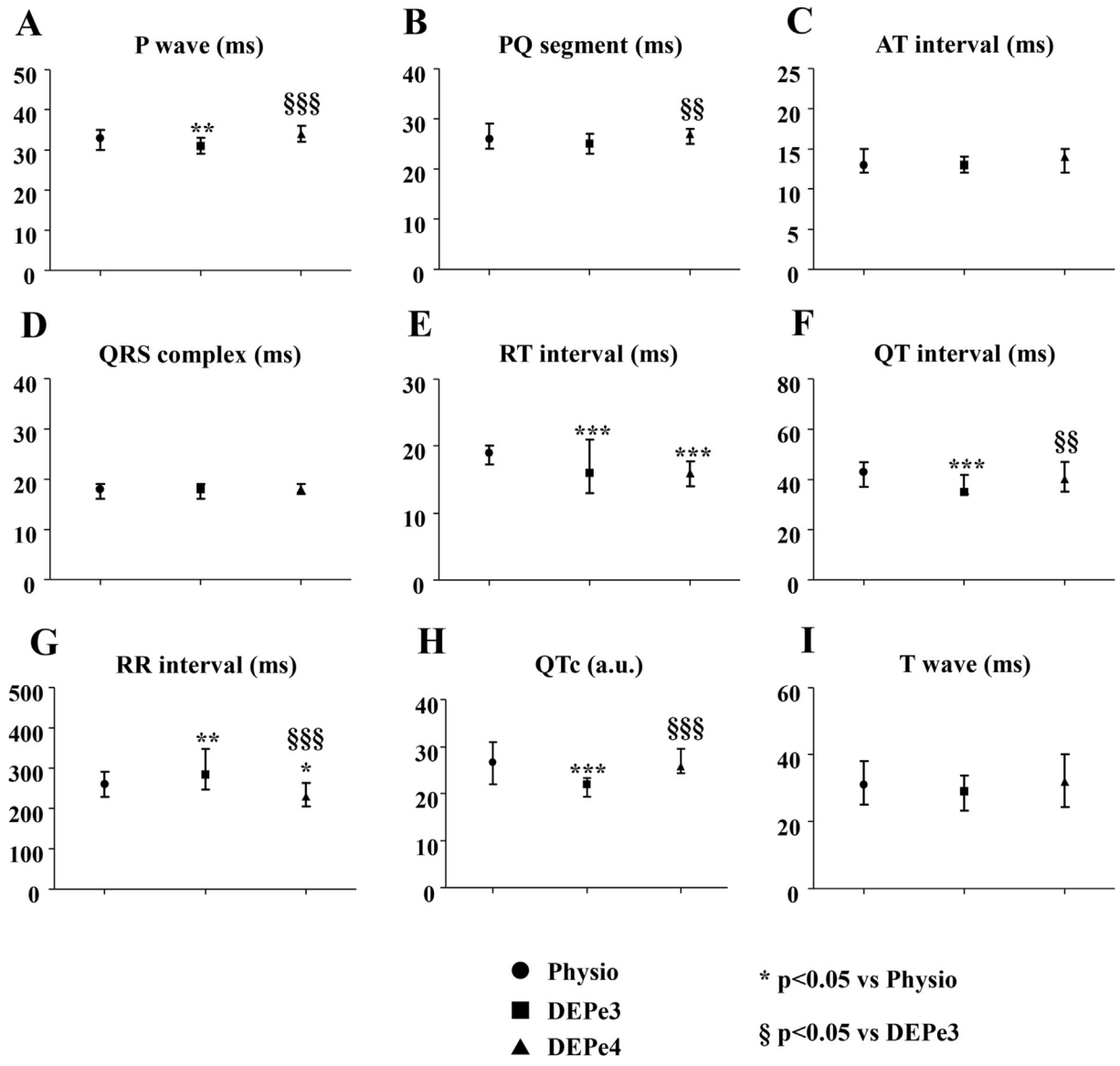

Fig. 3. Basic EG parameters evaluated in Physio (circle), DEPe3 (square) and DEPe4 (triangle) treated animals. **A**: P wave duration (ms). **B**: PQ segment duration (ms). **C**: AT interval duration (ms). **D**: QRS complex duration (ms). **E**: RT interval duration (ms). **F**: QT interval duration (ms). **G**: RR interval duration (ms). **H**: QTc duration (ms). **I**: T wave duration (ms). Kruskal-Wallis (post hoc analyses: Dunn's multiple comparison test). Statistical significance set at $p < 0.05$.

DEPe3 and by 56% in DEPe4.

3.3.5. Lipid peroxidation activity and inflammation

Lung tissue showed positive TBARS values, in both DEPe3 and DEPe4 animals, indicating membrane damage due to ROS production (Fig. 5A). In the cardiac tissue, lipid peroxidation is observed for both DEPs, indicating cell membrane damage (Fig. 5B). We did not observe any change related to inflammation for IL-6 and MCP-1 as well as for the tissue remodeling biomarkers MMP9 and TIMP-1 (Fig. S4).

4. Discussion

The results of the *in-vitro* data demonstrated that DEPe4, due to its natural enrichment in nanoparticles, has been rapidly internalized from cardiac cells without affecting cell survival. Such rapid internalization can jeopardize *in-vivo* conduction velocity acutely, and therefore increase arrhythmogenesis.

4.1. DEP physicochemical characterization

Raman spectra of DEP samples are in agreement with previous works on commercial carbon black. Carbon materials show two main Raman bands: the D (defect or disorder) band at about 1300–1350 cm^{-1} related to structural defects, disorder or impurities in carbon, associated with non-sp^2 bonds at the edge sites of particles (Sadezky et al., 2005) and the G (graphitic) band at about 1580-1600 cm^{-1} associated to vibrations involving planar sp2 C-C bonds. The non-sp2 bonds at the edge sites are easily involved during oxidation processes (Schmid et al., 2011).

D-band at around 1300 cm^{-1} and G-band at around 1600 cm^{-1} are the main features of carbon materials and have been explained as representing disorder-induced and graphitic features, respectively (Iqbal et al., 2012; Yun et al., 2013). Despite the apparent similarity of the Raman spectra (Fig. 1A), the ratio of the Intensities (areas) of the D and G bands shows a significant difference: $I_D/I_G = 2.4$ for DEPe3 and $I_D/I_G = 3.1$ for DEPe4.

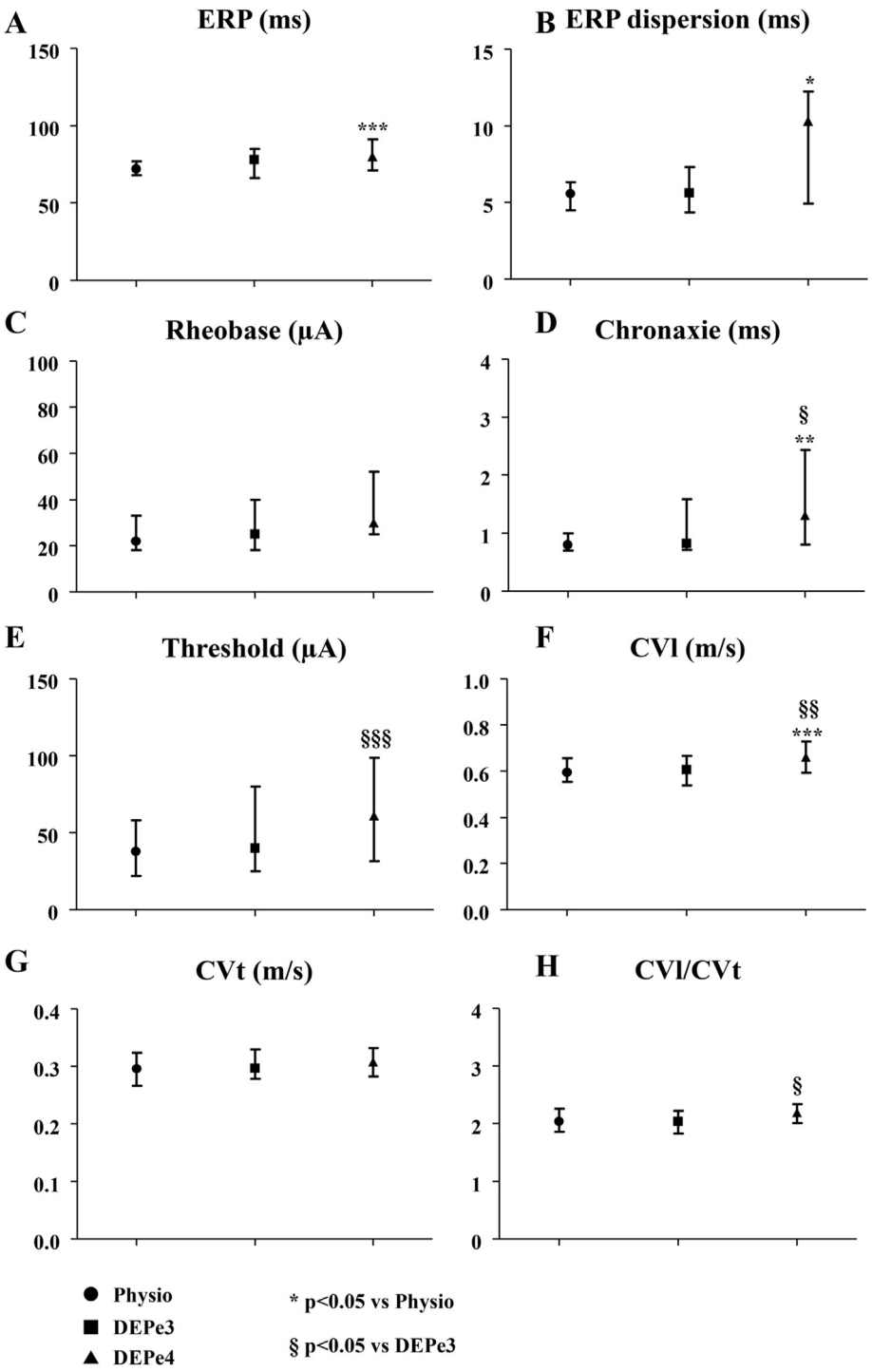

Fig. 4. Electrophysiological parameters in Physio (circle), DEPe3 (square) and DEPe4 (triangle) treated animals. **A**: Effective refractory period (ERP, ms). **B**: Cardiac refractoriness dispersion. **C**: Rheobase (μA). **D**: Chronaxie (ms). **E**: Threshold intensity for a 1 ms duration impulse (μA). **F**: Ventricular conduction velocities along to the fiber (CVl, m/s). **G**: Ventricular conduction velocities across to the fiber (CVt, m/s). **H**: Ventricular velocities ratio (CVl/CVt). Kruskal-Wallis (post hoc analyses: Dunn's multiple comparison test). Statistical significance set at $p < 0.05$.

The degree of graphitization of the DEPe4 samples, seems, therefore, lower than the corresponding one determined in DEPe3 material: the number of edge site carbon atoms concerning basal plane carbon atoms should correspond to greater reactivity of DEPe4 compared to DEPe3.

The chain-like agglomerates are composed of nearly-spherical basic units, namely primary soot nanoparticles (Dobbins et al., 1998). The size of DEPs is well represented by asymmetric-geometric distributions with an average dimensional of DEPe4 smaller (<150 μm) than DEPe3. DEPe4 is enriched with nano-particles compared to DEPe3. Indeed, DEPe3 of less than 150 nm was not been detected. In regards to metal characterization, Cr, Cu and Ni are two-timed higher in the DEPe3 vs. DEPe4 while Zn is ten-times higher in DEPe4. To the best of our knowledge, no clear

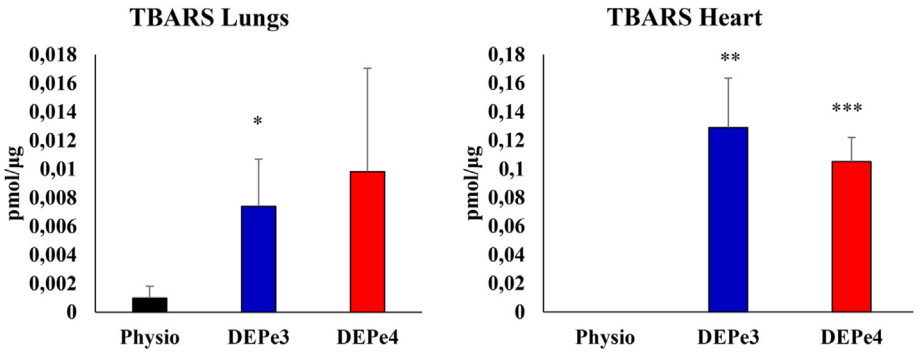

Fig. 5. Toxicological markers in lungs and heart. TBARS production evaluation in lungs (left, n = 8) and heart (right, n = 8) tissue. Blue bar: DEPe3; red bar: DEPe4. Kruskal-Wallis (post hoc analyses: Dunn's multiple comparison test). Statistical significance set at $p < 0.05$. (For interpretation of the references to colour in this figure legend, the reader is referred to the Web version of this article.)

relationship between metal composition and size distribution of particles has been yet demonstrated. In our previous study in a steelmaking foundry (Marcias et al., 2018), we found that Ni showed almost uniform distribution for all size ranges, whereas Cr showed high variation in the fraction size ranging from concentrations lower than the detection limit value (0.316 μm, 1.956 and 8.126) to about 30% (0.761 μm) of the total element in a single fraction. 62–77% of the total amount of Zn was detected in the size range between 0.316 μm and 1.231 μm.

Few studies suggested that different PM compounds may have different toxicity and consequent influence on morbidity. The risk of death has been also shown to increase when PM mass contained a higher proportion of aluminum, arsenic, sulfate, silicon, and nickel (Franklin et al., 2008). Moreover, the incidence of cardiovascular diseases was significantly different when the PM mass was high in bromine, chromium, nickel, and sodium, while mass high in arsenic, chromium, manganese, organic carbon, nickel, and sodium supporting the idea that particle from traffic exerts greater cardiovascular toxicity (Zanobetti et al., 2009). PM-associated water-soluble metals, including zinc, can be absorbed via the pulmonary vasculature upon deposition, potentially reaching cardiac tissue at high concentrations (Wallenborn et al., 2007) before sequestered in the liver. Kodavanti and coworkers reported that episodic inhalation exposure of rats to oil combustion PM containing water-soluble zinc caused a myocardial injury (Kodavanti et al., 2008). Chromium regulates the expression of genes involved in oxidative stress, calcium signaling, fatty acid degradation, carcinogenesis, and cell growth in A549 cells (Ye and Shi, 2001). Data by the He group showed that exposure to zinc NPs was associated with cytotoxicity to the same cells (He et al., 2017). In regards to the organic compounds, the amount of BTEX absorbed by DEP was higher than their environmental concentrations (Fustinoni et al., 2010; Miri et al., 2016), highlighting how the origin of BTEX in DEP is linked to the diesel combustion process. PHAs composition and concentrations in DEP are consistent with those reported in (Alves et al., 2015). Pioneer studies, in agreement with our findings, showed how BTEX inhalation influences ventricular arrhythmias (Magos et al., 1990), and subacute poisoning with BTEX caused disorders in repolarization and arrhythmia in rats (Morvai and Ungvary, 1979). More recently, occupational exposure to PHAs was associated with a dose-response decrease in heart rate variability (Li et al., 2012) suggesting an altered cardiac autonomic function (Lee et al., 2011).

4.2. DEPe4 vs. DEPe3 cytotoxicity

Low doses of DEP induced a significant decrease in membrane adhesion force and an intense change in A549 membrane stiffness over time, which were closely associated with changes in cell topography, ultrastructure, or cytoskeletal change, or denaturation (Wu et al., 2013). Our experimental data strongly support the idea that small size DEP is capable of inducing a functional activation of lung alveolar epithelial cells, also stimulating their production and release of proinflammatory cytokines (Mazzarella et al., 2007). Lack of differences in oxidative stress and lipid peroxidation for both *in-vitro* and *in-vivo* data suggests that both DEPs activated ROS production independently from the physicochemical characteristics of the particles (Wilson et al., 2018).

Although not relevant for human exposure (cf. Table S1), we selected 50 μg/ml (Lehmann et al., 2009) as the minimal dose capable to exert *in-vitro* an effect on cell viability in both lungs and heart cells. Our data also showed that 50 μg/ml (of DEPe3 or DEPe4) reduced survival fraction and increase lipid peroxidation; additionally, cardiac cells, in contrast with A549 cells, internalized more rapidly DEPe4 compared to DEPe3 suggesting a more pronounced biophysical activity of DEPe4 than DEPe3.

4.3. DEPe4 vs. DEPe3 pro-arrhythmogenicity

The dose we employed for the DEP *in-vivo* exposure has been used by Nemmar et al. (Nemmar et al., 2003, 2010) resulting in 700 μg of total deposition mass in the alveolar rat compartment (Table S1). We are aware that does not exist a specific DEP threshold level for human exposure. The OSHA recommends a respirable dust limit for the airborne concentration of 5 mg/m^3 while no relevant limit has been introduced by the NIOSH yet (https://www.cdc.gov/niosh/docs/88-116/). In our case, accounting for the limits of species-specificity and procedure (tracheal instillation vs the inhalation realistic scenario) we selected 2 mg/kg for the instilled dose (0.7 mg/kg, matching to 5 mg/m^3, 8h-TWA exert the same detrimental electrophysiological effect, data not shown) that could be taken into account in term of lifetime accumulating deposition. Electrocardiographic evaluation displayed different effects of DEPe3, compared to DEPe4, except for RT interval duration in which both treatments shorten cardiac repolarization. It seems that DEPe3 affects mainly cardiac electrophysiology, by impacting atrial activation time and ventricular repolarization. Theoretical simulation hypothesized that DEPs, depending on their aggregation level, can reach the alveolar compartment in the range of 4.7–27% of the inhaled dose (Sturm, 2017). These data are in agreement with our previous studies whereby NPs that overcome the blood/air barrier are capable to produce nanopores in cardiomyocytes (Miragoli et al., 2013) resulting in the development of leakage potassium currents that shortened the cardiac action potential and the RT

interval (Rossi et al., 2019; Savi et al., 2014). The increase in atrial excitability *in-vivo* is in line with previously described results (Helfenstein et al., 2008; Rossi et al., 2019) whereby nanopores slightly depolarized resting membrane potential which brings the tissue to the (pathological) point of supernormal conduction (Rohr et al., 1998). Both DEPe3 and DEPe4 treatment reduced ventricular cardiac excitability, even if DEPe4 displayed a more pronounced decrease. Excitability at the ventricular level displayed an opposite trend compared to atrial tissue that might be justified by the morphological and electrical differences between the tissues. Interestingly, an increase in ERP duration and ERP spatial dispersion – commonly recognized as a strong index of vulnerability to arrhythmia – was found only in DEPe4 (Fig. 5A and B). These data can be considered to go against the reduction of ventricular repolarization (RT interval), but the post-repolarization refractoriness can justify both parameters and is an important factor in determining unidirectional or bidirectional conduction block. Cardiac conduction velocity seems very similar becoming delayed only along fiber direction after DEPe4 treatment. Very interestingly conduction inhomogeneity was augmented in both treatments even if DEPe4 treatment displayed higher values. A local decrease in conduction velocity and a unidirectional conduction block are the conditions necessary for re-entry. Arrhythmia susceptibility was nearly doubled in DEPe4 animals where conduction inhomogeneity parameters were higher. Noteworthy, biophysical and electrophysiological data are analyzed acutely, 4 h before tracheal instillation. Therefore, while arrhythmias susceptibility is increased, we did not found changes in cytokines expression or tissue remodeling for both lungs and heart (cf. Fig. S4).

We understood that a direct comparison between human inhalation exposure and rat tracheal instillation is not straightforward because of species-specificity and exposure route issues (i.e., different particle distribution, clearance and dose rates). Instillation studies are not recommended to determine the particle deposition in the lungs that occurs following inhalation. As previously mentioned, tracheal instillation has been widely used to evaluate the potential adverse effects of a specific material or mixture in the lower respiratory tract. Therefore, we are aware that our *in vivo* model does not represent a direct surrogate of realistic inhalation exposure, but we firmly believe that it provides novel insight into DEPs potential effect evaluation, especially in terms of accumulating deposition over the lifetime, and it might prompt further and more finely calibrated inhalation studies.

5. Conclusions

This study evaluated an (electro)toxicological effect of DEP on cell lines and *in-vivo* rat hearts. The data suggest that the higher is the presence of NPs in the inhaled soot (DEPe4 vs. DEPe3), the greater is the possibility of NPs entering the bloodstream. These NPs can be rapidly internalized by the cardiac cells suggesting a modification of their electrical balance increasing the likelihood of *in-vivo* arrhythmogenesis. Future investigations are necessary to provide further insight into pathophysiological pathways and structural remodeling involved in acute and chronic (accumulating deposition) adverse effects. Nevertheless, this work demonstrated that DEPe4 enriched in nanoparticles increases the vulnerability to cardiac arrhythmias in rats.

CRediT author statement

Stefano Rossi: Conceptualization, Investigation, Writing original draft. **Andrea Buccarello:** Methodology, Investigation, Software. **Cristina Caffarra Malvezzi:** Investigation. **Silvana Pinelli:** Methodology, Validation. **Rossella Alinovi:** Methodology, Validation. **Amparo Guerrero Gerboles:** Investigation. **Giacomo Rozzi:** Investigation, Editing. **Fabio Leonardi:** Methodology, Validation, Resources. **Valentina Bollati:** Data curation, Writing-reviewing, Funding acquisition. **Giuseppe de Palma:** Data curation, Methodology, Validation, **Paola Lagonegro:** Investigation. **Francesca Rossi:** Investigation, Data curation. **Pier Paolo Lottici:** Investigation, Validation, Writing original draft. **Rosario Statello:** Investigation, Validation, Data curation. **Emilio Macchi:** Supervision. **Diana Poli:** Investigation, Data curation. **Michele Miragoli:** Conceptualization, Supervision, Funding acquisition, Writing-reviewing, Editing, Data curation. All authors have critically read and approved the final manuscript.

Data statements

All relevant data are included in the manuscript and supporting information and are also available from the authors upon request.

Funding

Italian Ministry of Health, Italy: GR-2009-1530528 to M.M.
Fondo Guido Erluison per la Ricerca Clinica, Dipartimento di Medicina e Chirurgia; postdoctoral salary to S.R.
Fondazione Fegato Scholarship 2017-2018 to C.C.M
PRIN 2015 INSIDE, GA: 20152T74ZL to V.B., M.M.

Declaration of competing interest

The authors declare that they have no known competing financial interests or personal relationships that could have appeared to influence the work reported in this paper.

Acknowledgments

We thank Riccardo Labadini, Enrica Gilberti and Giorgio Menna for their technical assistance. We thank Prof. Alberico Borghetti and Prof. Aderville Cabassi for the helpful discussion regarding the manuscript.

Appendix A. Supplementary data

Supplementary data to this article can be found online at https://doi.org/10.1016/j.envpol.2021.117163.

References

Alves, C.A., Barbosa, C., Rocha, S., Calvo, A., Nunes, T., Cerqueira, M., Pio, C., Karanasiou, A., Querol, X., 2015. Elements and polycyclic aromatic hydrocarbons in exhaust particles emitted by light-duty vehicles. Environ. Sci. Pollut. Res. Int. 22, 11526–11542.
Baulig, A., Sourdeval, M., Meyer, M., Marano, F., Baeza-Squiban, A., 2003. Biological effects of atmospheric particles on human bronchial epithelial cells. Comparison with diesel exhaust particles. Toxicol. Vitro 17, 567–573.
Bhatnagar, A., 2006. Environmental cardiology: studying mechanistic links between pollution and heart disease. Circ. Res. 99, 692–705.
Brook, R.D., Brook, J.R., Rajagopalan, S., 2003. Air pollution: the "Heart" of the problem. Curr. Hypertens. Rep. 5, 32–39.
Cesaroni, G., Forastiere, F., Stafoggia, M., Andersen, Z.J., Badaloni, C., Beelen, R., Caracciolo, B., de Faire, U., Erbel, R., Eriksen, K.T., Fratiglioni, L., Galassi, C., Hampel, R., Heier, M., Hennig, F., Hilding, A., Hoffmann, B., Houthuijs, D., Jockel, K.H., Korek, M., Lanki, T., Leander, K., Magnusson, P.K., Migliore, E., Ostenson, C.G., Overvad, K., Pedersen, N.L., J, J.P., Penell, J., Pershagen, G., Pyko, A., Raaschou-Nielsen, O., Ranzi, A., Ricceri, F., Sacerdote, C., Salomaa, V., Swart, W., Turunen, A.W., Vineis, P., Weinmayr, G., Wolf, K., de Hoogh, K., Hoek, G., Brunekreef, B., Peters, A., 2014. Long term exposure to ambient air pollution and incidence of acute coronary events: prospective cohort study and meta-analysis in 11 European cohorts from the ESCAPE Project. BMJ 348, f7412.
Cofala, J., Amann, M., Klimont, Z., Kupiainen, K., Hoglund-Isaksson, L., 2007. Scenarios of global anthropogenic emissions of air pollutants and methane until 2030. Atmos. Environ. 41, 8486–8499.

Cohen, A.J., Brauer, M., Burnett, R., Anderson, H.R., Frostad, J., Estep, K., Balakrishnan, K., Brunekreef, B., Dandona, L., Dandona, R., Feigin, V., Freedman, G., Hubbell, B., Jobling, A., Kan, H., Knibbs, L., Liu, Y., Martin, R., Morawska, L., Pope 3rd, C.A., Shin, H., Straif, K., Shaddick, G., Thomas, M., van Dingenen, R., van Donkelaar, A., Vos, T., Murray, C.J.L., Forouzanfar, M.H., 2017. Estimates and 25-year trends of the global burden of disease attributable to ambient air pollution: an analysis of data from the Global Burden of Diseases Study 2015. Lancet 389, 1907–1918.

Dias, P., Desplantez, T., El-Harasis, M.A., Chowdhury, R.A., Ullrich, N.D., Cabestrero de Diego, A., Peters, N.S., Severs, N.J., MacLeod, K.T., Dupont, E., 2014. Characterisation of connexin expression and electrophysiological properties in stable clones of the HL-1 myocyte cell line. PloS One 9, e90266.

Dobbins, R.A., Fletcher, R.A., Chang, H.C., 1998. The evolution of soot precursor particles in a diffusion flame. Combust. Flame 115, 285–298.

Dockery, D.W., Pope 3rd, C.A., Xu, X., Spengler, J.D., Ware, J.H., Fay, M.E., Ferris Jr., B.G., Speizer, F.E., 1993. An association between air pollution and mortality in six U.S. cities. N. Engl. J. Med. 329, 1753–1759.

Fox, J.R., Cox, D.P., Drury, B.E., Gould, T.R., Kavanagh, T.J., Paulsen, M.H., Sheppard, L., Simpson, C.D., Stewart, J.A., Larson, T.V., Kaufman, J.D., 2015. Chemical characterization and in vitro toxicity of diesel exhaust particulate matter generated under varying conditions. Air Qual Atmos Health 8, 507–519.

Franklin, M., Koutrakis, P., Schwartz, J., 2008. The role of particle composition on the association between PM2.5 and mortality. Epidemiology 19, 680–689.

Fustinoni, S., Rossella, F., Campo, L., Mercadante, R., Bertazzi, P.A., 2010. Urinary BTEX, MTBE and naphthalene as biomarkers to gain environmental exposure profiles of the general population. Sci. Total Environ. 408, 2840–2849.

Hazari, M.S., Haykal-Coates, N., Winsett, D.W., Krantz, Q.T., King, C., Costa, D.L., Farraj, A.K., 2011. TRPA1 and sympathetic activation contribute to increased risk of triggered cardiac arrhythmias in hypertensive rats exposed to diesel exhaust. Environ. Health Perspect. 119, 951–957.

He, T., Long, J.M., Li, J., Liu, L.L., Cao, Y., 2017. Toxicity of ZnO nanoparticles (NPs) to A549 cells and A549 epithelium in vitro: interactions with dipalmitoyl phosphatidylcholine (DPPC). Environ. Toxicol. Pharmacol. 56, 233–240.

Helfenstein, M., Miragoli, M., Rohr, S., Muller, L., Wick, P., Mohr, M., Gehr, P., Rothen-Rutishauser, B., 2008. Effects of combustion-derived ultrafine particles and manufactured nanoparticles on heart cells in vitro. Toxicology 253, 70–78.

Iodice, S., Hoxha, M., Ferrari, L., Carbone, I.F., Anceschi, C., Miragoli, M., Pesatori, A.C., Persico, N., Bollati, V., 2018. Particulate air pollution, blood mitochondrial DNA copy number, and telomere length in mothers in the first trimester of pregnancy: effects on fetal growth. Oxid Med Cell Longev 2018, 5162905.

Iqbal, M.W., Singh, A.K., Iqbal, M.Z., Eom, J., 2012. Raman fingerprint of doping due to metal adsorbates on graphene. J. Phys. Condens. Matter 24, 335301.

Karoui, A., Crochemore, C., Mulder, P., Preterre, D., Cazier, F., Dewaele, D., Corbiere, C., Mekki, M., Vendeville, C., Richard, V., Vaugeois, J.M., Fardel, O., Sichel, F., Lecureur, V., Monteil, C., 2019. An integrated functional and transcriptomic analysis reveals that repeated exposure to diesel exhaust induces sustained mitochondrial and cardiac dysfunctions. Environ. Pollut. 246, 518–526.

Kodavanti, U.P., Schladweiler, M.C., Gilmour, P.S., Wallenborn, J.G., Mandavilli, B.S., Ledbetter, A.D., Christiani, D.C., Runge, M.S., Karoly, E.D., Costa, D.L., Peddada, S., Jaskot, R., Richards, J.H., Thomas, R., Madamanchi, N.R., Nyska, A., 2008. The role of particulate matter-associated zinc in cardiac injury in rats. Environ. Health Perspect. 116, 13–20.

Lapuerta, Magin, 2019. Analysis of Soot from the Use of Butanol Blends in a Euro 6 Diesel Engine. Energy Fuels 33 (3), 2265–2277. https://doi.org/10.1021/acs.energyfuels.8b04083.

Lee, M.S., Magari, S., Christiani, D.C., 2011. Cardiac autonomic dysfunction from occupational exposure to polycyclic aromatic hydrocarbons. Occup. Environ. Med. 68, 474–478.

Lehmann, A.D., Blank, F., Baum, O., Gehr, P., Rothen-Rutishauser, B.M., 2009. Diesel exhaust particles modulate the tight junction protein occludin in lung cells in vitro. Part. Fibre Toxicol. 6, 26.

Li, X., Feng, Y., Deng, H., Zhang, W., Kuang, D., Deng, Q., Dai, X., Lin, D., Huang, S., Xin, L., He, Y., Huang, K., He, M., Guo, H., Zhang, X., Wu, T., 2012. The dose-response decrease in heart rate variability: any association with the metabolites of polycyclic aromatic hydrocarbons in coke oven workers? PloS One 7, e44562.

Liu, J., Ye, X., Ji, D., Zhou, X., Qiu, C., Liu, W., Yu, L., 2018. Diesel exhaust inhalation exposure induces pulmonary arterial hypertension in mice. Environ. Pollut. 237, 747–755.

Lucking, A.J., Lundback, M., Barath, S.L., Mills, N.L., Sidhu, M.K., Langrish, J.P., Boon, N.A., Pourazar, J., Badimon, J.J., Gerlofs-Nijland, M.E., Cassee, F.R., Boman, C., Donaldson, K., Sandstrom, T., Newby, D.E., Blomberg, A., 2011. Particle traps prevent adverse vascular and prothrombotic effects of diesel engine exhaust inhalation in men. Circulation 123, 1721–1728.

Magos, G.A., Lorenzana-Jimenez, M., Vidrio, H., 1990. Toluene and benzene inhalation influences on ventricular arrhythmias in the rat. Neurotoxicol. Teratol. 12, 119–124.

Mann, J.K., Tager, I.B., Lurmann, F., Segal, M., Quesenberry Jr., C.P., Lugg, M.M., Shan, J., Van Den Eeden, S.K., 2002. Air pollution and hospital admissions for ischemic heart disease in persons with congestive heart failure or arrhythmia. Environ. Health Perspect. 110, 1247–1252.

Marcias, G., Fostinelli, J., Catalani, S., Uras, M., Sanna, A.M., Avataneo, G., De Palma, G., Fabbri, D., Paganelli, M., Lecca, L.I., Buonanno, G., Campagna, M., 2018. Composition of metallic elements and size distribution of fine and ultrafine particles in a steelmaking factory. Int. J. Environ. Res. Publ. Health 15.

Mayer, A., Kasper, M., Czerwinski, J., 2014. Nanoparticle counts emissions of trucks: EURO 3 with and without DPF compared to EURO 4 and EURO 5. Energy Power 4, 1–10.

Mazzarella, G., Ferraraccio, F., Prati, M.V., Annunziata, S., Bianco, A., Mezzogiorno, A., Liguori, G., Angelillo, I.F., Cazzola, M., 2007. Effects of diesel exhaust particles on human lung epithelial cells: an in vitro study. Respir. Med. 101, 1155–1162.

Mills, N.L., Donaldson, K., Hadoke, P.W., Boon, N.A., MacNee, W., Cassee, F.R., Sandstrom, T., Blomberg, A., Newby, D.E., 2009. Adverse cardiovascular effects of air pollution. Nat. Clin. Pract. Cardiovasc. Med. 6, 36–44.

Miragoli, M., Ceriotti, P., Iafisco, M., Vacchiano, M., Salvarani, N., Alogna, A., Carullo, P., Ramirez-Rodriguez, G.B., Patricio, T., Esposti, L.D., Rossi, F., Ravanetti, F., Pinelli, S., Alinovi, R., Erreni, M., Rossi, S., Condorelli, G., Post, H., Tampieri, A., Catalucci, D., 2018. Inhalation of peptide-loaded nanoparticles improves heart failure. Sci. Transl. Med. 10.

Miragoli, M., Novak, P., Ruenraroengsak, P., Shevchuk, A.I., Korchev, Y.E., Lab, M.J., Tetley, T.D., Gorelik, J., 2013. Functional interaction between charged nanoparticles and cardiac tissue: a new paradigm for cardiac arrhythmia? Nanomedicine 8, 725–737.

Miri, M., Rostami Aghdam Shendi, M., Ghaffari, H.R., Ebrahimi Aval, H., Ahmadi, E., Taban, E., Gholizadeh, A., Yazdani Aval, M., Mohammadi, A., Azari, A., 2016. Investigation of outdoor BTEX: concentration, variations, sources, spatial distribution, and risk assessment. Chemosphere 163, 601–609.

Morvai, V., Ungvary, G., 1979. Effects of simultaneous alcohol and toluene poisoning on the cardiovascular system of rats. Toxicol. Appl. Pharmacol. 50, 381–389.

Nemmar, A., Al-Salam, S., Zia, S., Yasin, J., Al Husseni, I., Ali, B.H., 2010. Diesel exhaust particles in the lung aggravate experimental acute renal failure. Toxicol. Sci. 113, 267–277.

Nemmar, A., Hoet, P.H., Dinsdale, D., Vermylen, J., Hoylaerts, M.F., Nemery, B., 2003. Diesel exhaust particles in lung acutely enhance experimental peripheral thrombosis. Circulation 107, 1202–1208.

Nemmar, A., Hoet, P.H., Vanquickenborne, B., Dinsdale, D., Thomeer, M., Hoylaerts, M.F., Vanbilloen, H., Mortelmans, L., Nemery, B., 2002. Passage of inhaled particles into the blood circulation in humans. Circulation 105, 411–414.

Peretz, A., Kaufman, J.D., Trenga, C.A., Allen, J., Carlsten, C., Aulet, M.R., Adar, S.D., Sullivan, J.H., 2008a. Effects of diesel exhaust inhalation on heart rate variability in human volunteers. Environ. Res. 107, 178–184.

Peretz, A., Sullivan, J.H., Leotta, D.F., Trenga, C.A., Sands, F.N., Allen, J., Carlsten, C., Wilkinson, C.W., Gill, E.A., Kaufman, J.D., 2008b. Diesel exhaust inhalation elicits acute vasoconstriction in vivo. Environ. Health Perspect. 116, 937–942.

Peters, A., Dockery, D.W., Muller, J.E., Mittleman, M.A., 2001. Increased particulate air pollution and the triggering of myocardial infarction. Circulation 103, 2810–2815.

Rohr, S., Kucera, J.P., Kleber, A.G., 1998. Slow conduction in cardiac tissue, I: effects of a reduction of excitability versus a reduction of electrical coupling on microconduction. Circ. Res. 83, 781–794.

Rossi, S., Savi, M., Mazzola, M., Pinelli, S., Alinovi, R., Gennaccaro, L., Pagliaro, A., Meraviglia, V., Galetti, M., Lozano-Garcia, O., Rossini, A., Frati, C., Falco, A., Quaini, F., Bocchi, L., Stilli, D., Lucas, S., Goldoni, M., Macchi, E., Mutti, A., Miragoli, M., 2019. Subchronic exposure to titanium dioxide nanoparticles modifies cardiac structure and performance in spontaneously hypertensive rats. Part. Fibre Toxicol. 16, 25.

Sadezky, A., Muckenhuber, H., Grothe, H., Niessner, R., Poschl, U., 2005. Raman micro spectroscopy of soot and related carbonaceous materials: spectral analysis and structural information. Carbon 43, 1731–1742.

Samet, J.M., Dominici, F., Curriero, F.C., Coursac, I., Zeger, S.L., 2000. Fine particulate air pollution and mortality in 20 U.S. cities, 1987-1994. N. Engl. J. Med. 343, 1742–1749.

Savi, M., Rossi, S., Bocchi, L., Gennaccaro, L., Cacciani, F., Perotti, A., Amidani, D., Alinovi, R., Goldoni, M., Aliatis, I., Lottici, P.P., Bersani, D., Campanini, M., Pinelli, S., Petyx, M., Frati, C., Gervasi, A., Urbanek, K., Quaini, F., Buschini, A., Stilli, D., Rivetti, C., Macchi, E., Mutti, A., Miragoli, M., Zaniboni, M., 2014. Titanium dioxide nanoparticles promote arrhythmias via a direct interaction with rat cardiac tissue. Part. Fibre Toxicol. 11, 63.

Schmid, J., Grob, B., Niessner, R., Ivleva, N.P., 2011. Multiwavelength Raman microspectroscopy for rapid prediction of soot oxidation reactivity. Anal. Chem. 83, 1173–1179.

Steiner, S., Bisig, C., Petri-Fink, A., Rothen-Rutishauser, B., 2016. Diesel exhaust: current knowledge of adverse effects and underlying cellular mechanisms. Arch. Toxicol. 90, 1541–1553.

Sturm, R., 2017. Deposition of diesel exhaust particles in the human lungs: theoretical simulations and experimental data. J. Publ. Health Epidemiol. 1.

Su, D.S., Serafino, A., Muller, J.O., Jentoft, R.E., Schlogl, R., Fiorito, S., 2008. Cytotoxicity and inflammatory potential of soot particles of low-emission diesel engines. Environ. Sci. Technol. 42, 1761–1765.

Tanwar, V., Adelstein, J.M., Grimmer, J.A., Youtz, D.J., Sugar, B.P., Wold, L.E., 2017. PM2.5 exposure in utero contributes to neonatal cardiac dysfunction in mice. Environ. Pollut. 230, 116–124.

Uy, D., Ford, M.A., Jayne, D.T., O'Neill, A.E., Haack, L.P., Hangas, J., Jagner, M.J., Sammut, A., Gangopadhyay, A.K., 2014. Characterization of gasoline soot and comparison to diesel soot: morphology, chemistry, and wear. Tribol. Int. 80, 198–209.

Wallenborn, J.G., McGee, J.K., Schladweiler, M.C., Ledbetter, A.D., Kodavanti, U.P., 2007. Systemic translocation of particulate matter-associated metals following

a single intratracheal instillation in rats. Toxicol. Sci. 98, 231–239.
Weitekamp, C.A., Kerr, L.B., Dishaw, L., Nichols, J., Lein, M., Stewart, M.J., 2020. A systematic review of the health effects associated with the inhalation of particle-filtered and whole diesel exhaust. Inhal. Toxicol. 32, 1–13.
Wilson, S.J., Miller, M.R., Newby, D.E., 2018. Effects of diesel exhaust on cardiovascular function and oxidative stress. Antioxidants Redox Signal. 28, 819–836.
Wu, N., Lu, B., Chen, J., Li, X., 2021. Size distributions of particle-generated hydroxyl radical (.OH) in surrogate lung fluid (SLF) solution and their potential sources. Environ. Pollut. 268, 115582.
Wu, Y.Z., McEwen, G.D., Tang, M.J., Yu, T., Dimmick, J.T., Zhou, A.H., Gilbertson, T.A., Coulombe, R.A., Stevens, J.R., 2013. Sensing biophysical alterations of human lung epithelial cells (A549) in the context of toxicity effects of diesel exhaust particles. Cell Biochem. Biophys. 67, 1147–1156.
Ye, J.P., Shi, X.L., 2001. Gene expression profile in response to chromium-induced cell stress in A549 cells. Mol. Cell. Biochem. 222, 189–197.
Yun, K.S., Kim, B.R., Kang, W.S., Jung, S.C., Myung, S.T., Kim, S.J., 2013. Preparation of carbon blacks by liquid phase plasma (LPP) process. J. Nanosci. Nanotechnol. 13, 7381–7385.
Zanobetti, A., Franklin, M., Koutrakis, P., Schwartz, J., 2009. Fine particulate air pollution and its components in association with cause-specific emergency admissions. Environ. Health 8, 58.